

Exfoliation of self-assembled 2D organic-inorganic perovskite semiconductors

Wendy Niu,^{1,a)} Anna Eiden,² G. Vijaya Prakash,³ and Jeremy J. Baumberg¹

¹NanoPhotonics Centre, Cavendish Laboratory, University of Cambridge, Cambridge CB3 0HE, United Kingdom

²Cambridge Graphene Centre, Engineering Department, University of Cambridge, 9, JJ Thomson Avenue, Cambridge CB3 0FA, United Kingdom

³Nanophotonics Lab, Department of Physics, Indian Institute of Technology Delhi, New Delhi 110016, India

(Received 10 March 2014; accepted 21 April 2014; published online 1 May 2014)

Ultra-thin flakes of 2D organic-inorganic perovskite ($C_6H_9C_2H_4NH_3$)₂PbI₄ are produced using micromechanical exfoliation. Mono- and few-layer areas are identified using optical and atomic force microscopy, with an interlayer spacing of 1.6 nm. Refractive indices extracted from the optical spectra reveal a sample thickness dependence due to the charge transfer between organic and inorganic layers. These measurements demonstrate a clear difference in the exciton properties between “bulk” (>15 layers) and very thin (<8 layer) regions as a result of the structural rearrangement of organic molecules around the inorganic sheets. © 2014 Author(s). All article content, except where otherwise noted, is licensed under a Creative Commons Attribution 3.0 Unported License. [<http://dx.doi.org/10.1063/1.4874846>]

The family of metal halide based organic-inorganic perovskites have been extensively studied for their optical and electrical properties.^{1–15} Recently, 3D perovskites of the form $CH_3NH_3PbI_{3-x}Cl_x$ have been used to produce solar cells with efficiencies of up to 15%.^{1–4} 2D lead iodide (PbI) perovskites have also received a great deal of attention as self-assembling multiple quantum well structures with exciton binding energies in excess of 200 meV.^{5–7} Such systems are built from monolayers of corner-sharing PbI₆ octahedra sandwiched between organic molecular layers. The 3D structure is formed by stacking these sheets, with van der Waals forces acting between neighbouring organic molecules. Quantum and dielectric confinement of excitons in the inorganic sheets create room temperature excitons with high oscillator strength. A wide range of controllable processing methods are available to lay down such films, for example, spin coating,^{8–10} layer-by-layer deposition,^{11,12} or intercalation of organic molecules into PbI₂ structures.^{13–15} Thus, 2D PbI perovskites are promising candidates for use as active materials in optoelectronic devices.

In recent years, much attention has been paid to 2D layered compounds such as graphene or transition metal dichalcogenides. Due to weak van der Waals bonding, it is easy to cleave neighbouring layers and form ultra-thin samples.^{16–21} In these materials, new optical and electronic properties emerge for mono- or few-layer regions, providing new avenues for material application. Here, we report micromechanical exfoliation of 2D PbI perovskites and explore the few-layer behaviour of such systems via optical spectroscopy.

Lead iodide (PbI₂) microcrystals are synthesized using a previously described solvothermal method, and intercalated using an organic ammonium iodide/toluene solution to create hexagonal ($C_6H_9C_2H_4NH_3$)₂PbI₄ (CHPI) microcrystals ~30 μm in lateral size.¹⁵ We then use a micromechanical exfoliation technique to create thinner flakes, transferring the

resulting samples onto an oxidized silicon (Si) wafer for further measurements. The thinnest regions are identified using optical microscopy, and then characterized with white light spectroscopy and atomic force microscopy (AFM).

Bright field (BF) and dark field (DF) reflection images of a typical CHPI flake are shown at 100× magnification in Figs. 1(a) and 1(b), respectively. The DF scattering seen from the edges and grain boundaries of the sample is typical for such crystals. The reflectivity spectra for these exfoliated samples [Fig. 1(d)] consist of an excitonic Fano resonance at $\lambda_{ex} \approx 504$ nm superimposed on a background of Fabry-Perot fringes. These fringes correspond to the colour of the crystal seen in BF and come from the path difference experienced by light double passing through the flake. The oxide layer on the substrate is designed to maximize optical contrast for very thin layers, and while optimized for graphene, this 280 nm SiO₂/Si system also works well for CHPI. By using this spectral information in conjunction with AFM measurements [Fig. 1(e)], we can correlate the position of Fabry-Perot fringes with thickness t . Thus, it is then possible to spectroscopically determine the thickness of CHPI flakes.

A histogram of AFM heights in the boxed area of Fig. 1(c) shows three predominant thicknesses, which can be fit to Gaussians separated by steps of 1.6 nm [Fig. 1(f)]. This interlayer spacing agrees well with X-ray diffraction measurements, where the periodicity was found to be 1.7–1.8 nm.^{13,22} Due to the presence of molecules adsorbed on the surface of the substrate, the initial step of 2.5 nm is likely due to a monolayer, allowing us to label the three peaks as 1-, 2-, and 3-layer regions.

Spectroscopic measurements of flake thickness require detailed knowledge of the CHPI refractive index, which is not well known. Instead, we extract the required information from reflectivity data using the transfer matrix formulation.²³ In the wavelength range of interest (460–750 nm), the dielectric function ϵ of 2D PbI perovskites can be modelled as the sum of a constant background and two Lorentzian oscillators: the

^{a)}Electronic mail: wwn20@cam.ac.uk



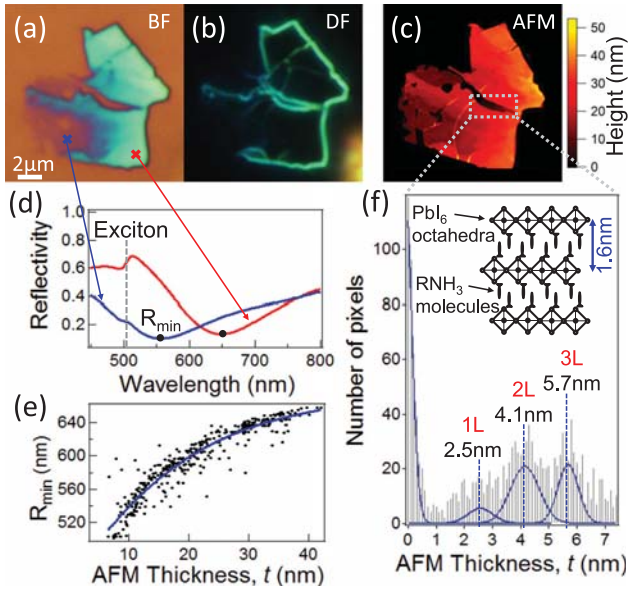


FIG. 1. Images in $100\times$ magnification using (a) bright and (b) dark field on an exfoliated CHPI flake; (c) AFM image of the same area. (d) Reflectivity spectra of two regions on the flake. The exciton wavelength is indicated by the dashed line. (e) Relationship between the measured reflectivity minimum (labelled as R_{\min} in (d)) and AFM thickness. (f) Histogram of heights measured in the boxed area of (c). Multipole fitting to the data (blue lines) gives an interlayer spacing of 1.6 nm. The inset shows the structure of 2D PbI₂ perovskites.

exciton (*ex*) and an additional charge transfer (*CT*) transition at ~ 400 nm.^{9,10,24–27} Hence

$$\epsilon = \epsilon_1 + i\epsilon_2 + \frac{A_{ex}}{\lambda_{ex}^2 - \lambda^2 + i\Gamma_{ex}\lambda} + \frac{A_{CT}}{\lambda_{CT}^2 - \lambda^2 + i\Gamma_{CT}\lambda}, \quad (1)$$

where ϵ_1, ϵ_2 are the background terms, while A_i is the amplitude, λ_i is the wavelength, and Γ_i is the linewidth of oscillator i . The refractive index ($\tilde{n} = \sqrt{\epsilon}$) can then be used in the multilayer transfer matrix to calculate the expected reflectivity. The *CT* peak, due to the charge transfer between organic and inorganic layers, is particularly sensitive to disorder and depends on the precise spin coating conditions when comparable thin films are produced.⁹

The results of these refractive index fits for more than 200 spectra are shown in Fig. 2. The fitting works well for spectra that are not collected at the edges of the flake; therefore, the thinnest areas are excluded. Within these regions, two main regimes of refractive index are observed. In both cases, the background and exciton oscillator are relatively unchanged. For thicker areas of the sample ($t \geq 25$ nm), a low-absorption regime is observed, where the *CT* oscillator is mainly reflective. For thinner areas ($t \sim 10 - 25$ nm), a high-absorption regime is seen, where the *CT* oscillator redshifts and becomes more optically active. As discussed below, the thickness range encompassed by the absorbing regime is correlated with a region of structural reconfiguration. This leads to a change in the energy states of the hybrid perovskite and modifies the charge transfer between neighbouring organic and inorganic sheets. For comparison, the refractive index of a $t \sim 60$ nm film extracted from ellipsometry (grey dashed line) is also shown in Fig. 2. The film

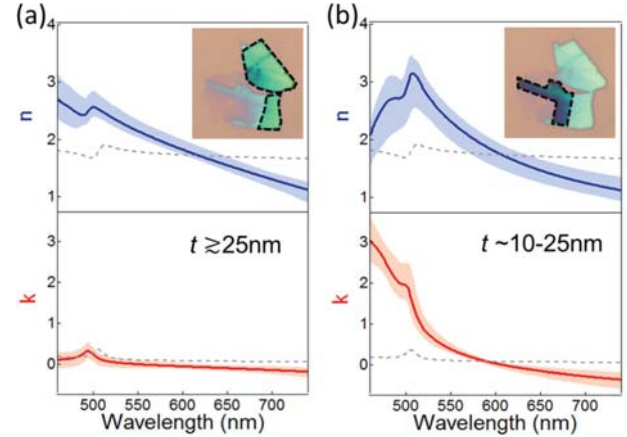


FIG. 2. Fitted complex refractive index of CHPI flakes for more than 200 pixels. Two regimes are found: (a) low absorption, occurring at positions of high thickness ($t \geq 25$ nm), and (b) high absorption, at lower thickness ($t \sim 10 - 25$ nm). The insets indicate typical areas where each regime is found. Shaded regions show the range of values extracted from the fit, and grey dotted lines represent the refractive index of a CHPI film ($t \sim 60$ nm) measured using ellipsometry.

absorption (k) is closer to that of thicker flake areas, with a reduced contribution from the *CT* oscillator in the refractive index. X-ray diffraction shows that while distinct layers are formed during spin coating, there is greater structural disorder in each layer when compared with intercalated PbI₂ microcrystals.¹⁵ This interface mismatch can be responsible for a large range of charge transfer environments, leading to the reduced strength of the *CT* resonance that we observe here.

In reflectivity, the exciton produces a Fano lineshape due to interference between its narrow resonance and the continuum background. On account of this complication, we extract information about exciton properties by describing $\Delta R = R_{\text{CHPI}} - R_{\text{substrate}}$ as

$$\Delta R = R_{bkg} + A \frac{(\lambda - \lambda_{ex} + q\gamma)^2}{(\lambda - \lambda_{ex})^2 + \gamma^2}, \quad (2)$$

where R_{bkg} represents the continuum background with Fabry-Perot fringing; A , λ_{ex} , and γ are the amplitude, wavelength, and linewidth of the exciton, respectively, and the parameter q describes the asymmetric shape of the Fano resonance. The results of the fit are shown in Fig. 3 for positions across many flakes with different thicknesses. A , λ_{ex} , and γ are equivalent to the corresponding terms in Eq. (1), while q represents the interference between the exciton, *CT*, and background terms. Near the vicinity of the exciton, the effects of the *CT* and background are not distinguished; therefore, Eq. (2) allows us to focus exclusively on the exciton components, while Eq. (1) gives us the overall refractive index. Since the perovskite resembles a multilayer system, we find the exciton amplitude initially scales linearly with the number of layers as expected, before saturating at $t \approx 27$ nm (15 layers). The large variability of amplitudes at high thickness arises predominantly from spectra taken at edges of flakes. Linear extrapolation of our data indicates the exciton amplitude will drop to zero at $t \sim 7$ nm (3 layers). However, layer-by-layer assembly of perovskite films has

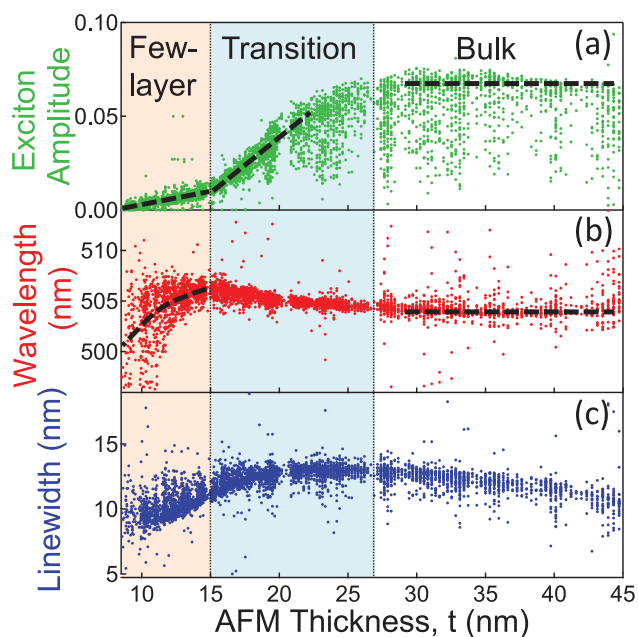


FIG. 3. Fitted exciton (a) amplitude, (b) wavelength, and (c) linewidth from reflectivity spectra (see Eq. (2)). Dashed lines are guides for the eye.

shown that linear increases in the exciton intensity occur only after the fourth layer, while two monolayers are required to observe room temperature exciton behaviour.¹²

From Fig. 3, we identify 3 regions of interest. First, the “bulk” region ($t \geq 27$ nm), where the exciton wavelength remains roughly constant; second, the transition region ($t \sim 15 - 27$ nm), where the wavelength begins to redshift, while the linewidth reaches a maximum; and finally, the few-layer region, where the wavelength blueshifts below the bulk limit, along with a decrease in the linewidth. These data help us to understand the changes happening at a structural level: disorder causes inhomogeneous broadening of the exciton resonance,^{28–30} while the exciton energy is directly related to the angle between PbI_6 octahedra in the inorganic layers.⁸ In “bulk” CHPI, the exciton has a wavelength of 504 nm and a spectral width of ≈ 10 nm. Close to the thickness transition region, the system is seen to become more disordered as the PbI sheets rearrange, becoming flatter, and more strained. Finally, at small t , the few-layer regime reveals how the layers relax and crumple again to reach the lowest energy configuration. Extrapolation of the fitted exciton wavelength to monolayer thickness (3 nm) leads to a wavelength of ~ 495 nm, comparable to the value of ~ 490 nm reported for PbI_2 thin films.^{31,32} We were unable to spectroscopically probe areas with $t < 8$ nm (4 layers) as they lie on the edges of flakes and are around 100 nm in size. Since the lateral resolution of reflectivity measurements is $1 \mu\text{m}$, these spectra are averaged with the much bigger signals from thicker areas. In order to achieve more sizeable monolayer regions, large-area samples are desirable for exfoliation, for instance, using solution-grown single crystals. Exfoliating onto flexible polymer substrates may also improve our capability for attaining large monolayer regions as this can reduce fracture of crystals. However, our measurements clearly show that these organic-inorganic hybrid perovskites change their electronic properties as the thickness is reduced, and

this is connected to changes in the strain, disorder, and layer structure.

In conclusion, we report the exfoliation of 2D organic-inorganic perovskites. Monolayers are observed, and the interlayer distance was found to be 1.6 nm. As with other 2D materials, the thinnest regions (< 8 layers) behave differently from the bulk material due to the influence of strain on the layer structure. We note however that the active excitonic layers are already electronically isolated in these hybrids, so changes in the band structure as observed in dichalcogenide systems are not expected. Instead, the effects seen are due to the re-organisation of organic molecules around the inorganic sheets. This suggests that pre-organisation of the intercalating molecules is key to controlling material structure at the monolayer scale, which may be accessible through chemical growth rather than exfoliation. This work suggests the potential to construct optoelectronic devices for monolayers of these hybrid materials, offering new routes to emission.

This work is part of the UK-India Education Research Initiative (UKIERI) and supported by EPSRC Grant Nos. EP/G060649/1, EP/H027130/1, and EU LINASS 320503. The authors would like to thank S. Ahmad for providing the inorganic microcrystals, and M. Barbone for help with AFM measurements.

¹H. S. Kim, C. R. Lee, J. H. Im, K. B. Lee, T. Moehl, A. Marchioro, S. J. Moon, R. Humphry-Baker, J. H. Yum, J. E. Moser, M. Grätzel, and N. G. Park, *Sci. Rep.* **2**, 591 (2012).

²M. M. Lee, J. Teuscher, T. Miyasaka, T. N. Murakami, and H. J. Snaith, *Science* **338**, 643 (2012).

³J. H. Heo, S. H. Im, J. H. Noh, T. N. Mandal, C. S. Lim, J. A. Chang, Y. H. Lee, H. Jung Kim, A. Sarkar, M. K. Nazeeruddin, M. Grätzel, and S. I. Seok, *Nat. Photonics* **7**, 486 (2013).

⁴M. Liu, M. B. Johnston, and H. J. Snaith, *Nature* **501**, 395 (2013).

⁵T. Ishihara, J. Takahashi, and T. Goto, *Phys. Rev. B* **42**, 11099 (1990).

⁶K. Tanaka, F. Sano, T. Takahashi, T. Kondo, R. Ito, and K. Ema, *Solid State Commun.* **122**, 249 (2002).

⁷K. Tanaka, T. Takahashi, T. Kondo, and K. Ema, *Phys. Rev. B* **71**, 045312 (2005).

⁸K. Pradeesh, J. J. Baumberg, and G. Vijaya Prakash, *Appl. Phys. Lett.* **95**, 173305 (2009).

⁹G. Vijaya Prakash, K. Pradeesh, R. Ratnani, K. Saraswat, M. E. Light, and J. J. Baumberg, *J. Phys. D: Appl. Phys.* **42**, 185405 (2009).

¹⁰S. Zhang, P. Audebert, Y. Wei, A. Al Choueiry, G. Lanty, A. Bréhier, L. Galmiche, G. Clavier, C. Boissière, J. S. Lauret, and E. Deleporte, *Materials* **3**, 3385 (2010).

¹¹M. Era and S. Oka, *Thin Solid Films* **376**, 232 (2000).

¹²T. Matsui, A. Yamaguchi, Y. Takeoka, M. Rikukawa, and K. Sanui, *Chem. Commun.* **3**, 1094 (2002).

¹³K. Pradeesh, J. J. Baumberg, and G. Vijaya Prakash, *Appl. Phys. Lett.* **95**, 033309 (2009).

¹⁴M. Era and K. Maeda, *Thin Solid Films* **331**, 285 (1998).

¹⁵I. Saikumar, S. Ahmad, J. J. Baumberg, and G. Vijaya Prakash, *Scr. Mater.* **67**, 834 (2012).

¹⁶K. S. Novoselov, A. K. Geim, S. V. Morozov, D. Jiang, Y. Zhang, S. V. Dubonos, I. V. Grigorieva, and A. A. Firsov, *Science* **306**, 666 (2004).

¹⁷P. Blake, E. W. Hill, A. H. Castro Neto, K. S. Novoselov, D. Jiang, R. Yang, T. J. Booth, and A. K. Geim, *Appl. Phys. Lett.* **91**, 063124 (2007).

¹⁸Z. H. Ni, H. M. Wang, J. Kasim, H. M. Fan, T. Yu, Y. H. Wu, Y. P. Feng, and Z. X. Shen, *Nano Lett.* **7**, 2758 (2007).

¹⁹A. Splendiani, L. Sun, Y. Zhang, T. Li, J. Kim, C. Y. Chim, G. Galli, and F. Wang, *Nano Lett.* **10**, 1271 (2010).

²⁰A. Castellanos-Gomez, N. Agrait, and G. Rubio-Bollinger, *Appl. Phys. Lett.* **96**, 213116 (2010).

²¹P. Tonndorf, R. Schmidt, P. Bottger, X. Zhang, J. Borner, A. Liebig, M. Albrecht, C. Kloc, O. Gordan, D. Zahn, S. de Vasconcellos, and R. Bratschitsch, *Opt. Express* **21**, 4908 (2013).

- ²²D. G. Billing and A. Lemmerer, *Acta Crystallogr., Sect. C: Cryst. Struct. Commun.* **62**, 269 (2006).
- ²³M. Born and E. Wolf, *Principles of Optics: Electromagnetic Theory of Propagation, Interference and Diffraction of Light*, 7th ed. (Cambridge University Press, 1999).
- ²⁴J. Fujisawa and T. Ishihara, *Phys. Rev. B* **70**, 113203 (2004).
- ²⁵J. Fujisawa and N. Tajima, *Phys. Rev. B* **72**, 125201 (2005).
- ²⁶J. Fujisawa, N. Tajima, K. Tamaki, M. Shimomura, and T. Ishihara, *J. Phys. Chem. C* **111**, 1146 (2007).
- ²⁷D. B. Mitzi, K. Chondroudis, and C. R. Kagan, *Inorg. Chem.* **38**, 6246 (1999).
- ²⁸S. Baranovskii, U. Doerr, and P. Thomas, *Phys. Rev. B* **48**, 17149 (1993).
- ²⁹L. Andreani and G. Panzarini, *Phys. Rev. B* **57**, 4670 (1998).
- ³⁰I. Kuznetsova, N. Gogh, J. Förstner, T. Meier, S. T. Cundiff, I. Varga, and P. Thomas, *Phys. Rev. B* **81**, 075307 (2010).
- ³¹T. Iwasaki, T. Goto, and Y. Nishina, *Phys. Status Solidi B* **88**, 289 (1978).
- ³²T. Goto and J. Maeda, *J. Phys. Soc. Jpn.* **56**, 3710 (1987).